Applied Radiation and Isotopes 103 (2015) 15–24

Contents lists available at ScienceDirect

Applied Radiation and Isotopes

journal homepage: www.elsevier.com/locate/apradiso

Identifying key surface parameters for optical photon transport in GEANT4/GATE simulations

Jenny Nilsson [a,*], Vesna Cuplov [b], Mats Isaksson [a]

[a] The Department of Radiation Physics, Institute of Clinical Sciences, The Sahlgrenska Academy, University of Gothenburg, Gula stråket 2B, 413 45 Göteborg, Sweden

[b] Institute of Nuclear Medicine, University College London Hospitals, Euston Road, London, United Kingdom

HIGHLIGHTS

- A comprehensive study of coupled ionizing particle and optical photon transport.
- A detailed description of the optical photon transport model in GEANT4/GATE.
- Scintillators used for spectrometry.
- The impact of optical photon transport on energy resolution.

ARTICLE INFO

Article history:
Received 23 January 2015
Received in revised form
24 March 2015
Accepted 28 April 2015
Available online 22 May 2015

Keywords:
Optical transport
Surface parameters
GEANT4
Energy resolution
Spectrometry
Whole body counting

ABSTRACT

For a scintillator used for spectrometry, the generation, transport and detection of optical photons have a great impact on the energy spectrum resolution. A complete Monte Carlo model of a scintillator includes a coupled ionizing particle and optical photon transport, which can be simulated with the GEANT4 code. The GEANT4 surface parameters control the physics processes an optical photon undergoes when reaching the surface of a volume. In this work the impact of each surface parameter on the optical transport was studied by looking at the optical spectrum: the number of detected optical photons per ionizing source particle from a large plastic scintillator, i.e. the output signal. All simulations were performed using GATE v6.2 (GEANT4 Application for Tomographic Emission). The surface parameter finish (polished, ground, front-painted or back-painted) showed the greatest impact on the optical spectrum whereas the surface parameter σ_α, which controls the surface roughness, had a relatively small impact. It was also shown how the surface parameters reflectivity and reflectivity types (specular spike, specular lobe, Lambertian and backscatter) changed the optical spectrum depending on the probability for reflection and the combination of reflectivity types. A change in the optical spectrum will ultimately have an impact on a simulated energy spectrum. By studying the optical spectra presented in this work, a GEANT4 user can predict the shift in an optical spectrum caused be the alteration of a specific surface parameter.

1. Introduction

Scintillation detectors have a wide field of applications and are found in areas such as radiation protection, portal monitoring, cosmic ray research or medical imaging. When an ionizing particle deposits energy in a scintillating material, electrons are excited and the relaxation of the excited states results in an emission of optical photons. The optical photons are transported through the scintillator and converted into an electric signal by an attached photodiode or a photomultiplier tube (PMT). The physics processes from the initial energy deposition to the output signal will significantly affect the energy resolution.

A scintillator energy spectrum can be computed by simulating the energy deposition only. An energy broadening function (GATE, 2013; Pelowitz, 2008) is then used to account for the influence of the physics processes occurring after energy deposition. An energy broadening function is a suitable option if the energy resolution is directly linked to the energy deposition. However, the number of detected optical photons by a photodiode or PMT depends not only on the energy deposition and scintillation yield but also on the

* Corresponding author.
E-mail address: jenny.nilsson@radfys.gu.se (J. Nilsson).

http://dx.doi.org/10.1016/j.apradiso.2015.04.017
0969-8043/

scintillator material, bulk absorption and the surface properties of the scintillator. The importance of transporting both ionizing particles and optical photons was shown in a recent work (Nilsson and Isaksson, 2015) where a whole body counter (WBC) (Nilsson and Isakkson, 2014) was Monte Carlo calibrated using ICRP:s (International Commission on Radiological Protection) computational phantoms (International Commission on Radiological Protection, 2009). In Ref. Nilsson and Isaksson (2015) GATE (GEANT4 Application for Tomographic Emission (GATE, 2013; Jan et al., 2004, 2011)) was used to simulate the transport of both ionizing particles and optical photons, which resulted in a good agreement between simulated and experimental energy spectrum.

GATE is an advanced open-source software that uses the GEANT4 libraries. Two optical simulation models are available in GEANT4 (GEANT4, 2012a), the GLISUR model and the UNIFIED model, but only the UNIFIED model is included in GATE. The UNIFIED model, developed by Levin and Moisan (Levin and Moisan, 1997), describes the physics processes an optical photon undergoes at a dielectric surface with respect to the surface properties. In an optical simulation the user defines the scintillator properties, such as scintillation yield and absorption length, as well as optical properties of all materials and surfaces. Surface properties are defined by a set of parameters and even though several articles on optical simulations in GATE and/or GEANT4 have been published (references are given in the discussion) an overview of all surface parameters and their individual and/or combined impact with respect to an energy spectrum have not been found. The aim of this article is to show how optical transport influences the energy resolution and to identify the key surface parameters in an optical simulation.

In this work all simulations were made for a large plastic scintillator, used in the WBC presented in Ref. Nilsson and Isaksson (2015). All surface parameters control physics processes that are independent of the scintillator size and material properties and hence the results from this work can be applicable for both inorganic and organic scintillators of different sizes and shapes.

2. Theory – optical photon transport in GATE

When using GATE for optical simulations, the user must define all material and surface properties (GATE, 2013; GEANT4, 2012a, 2012b). Material properties control the generation of optical photons (scintillation and fluorescence) and their transport through matter (Mie/Rayleigh scattering and bulk absorption). Surface properties control the physics processes (surface absorption, reflection or refraction) an optical photon undergoes when reaching a surface/boundary between two volumes.

This work describes a scintillator, defined by the following material properties:

- Scintillation yield: the expectation value of the Gaussian distributed number of emitted optical photons per energy deposition in the scintillator.
- Resolution scale: the standard deviation of the scintillation yield is given by resolution scale $\times$ (absorbed energy $\times$ scintillation yield)$^{1/2}$.
- Fast and slow time constants: the scintillation exponential decay time constants.
- Yield ratio: the fraction of the fast component relative to the total scintillation yield.

The material properties that control optical transport are

- Absorption length: the mean distance travelled by an optical photon before being bulk absorbed.
- Mie/Rayleigh scattering parameters: Mie scattering is the analytical solution of Maxwell's equations for scattering of optical photons by spherical particles. It is of importance only when the radius of the spherical particle is in the order of the optical photon wavelength. If the spherical particle is smaller than the optical photon wavelength the Mie scattering theory reduces to the Rayleigh approximation. Rayleigh scattering is an elastic scattering in which the optical photon changes direction without energy loss.
- Refractive index for the material.

The surface parameters are

- Type: defines if the surface is between two dielectric materials or one metal and one dielectric material. The surface between two dielectric materials can absorb, reflect or refract an optical photon whereas a surface between one dielectric and one metallic material can only absorb or reflect an optical photon.
- Finish: defines the structure of the surface and can be set to ground (G), polished (P), ground-front-painted (GFP), polished-front-painted (PFP), ground-back-painted (GBP) or polished-back-painted (PBP).
- Sigmaalpha (σ_α): defines the roughness of a surface.
- Surface refractive index: for GBP and PBP a refractive index needs to be defined. This should not be confused with the material refractive index. GBP and PBP describe a coated scintillator where there is a gap between the scintillator and the coating; the surface refractive index is the refractive index for the material in the gap.
- Efficiency: the probability of detecting an optical photon at a surface.
- Reflectivity (R): the probability for an optical photon to be reflected or refracted at a surface.
- Reflectivity type: defines the probability for a reflected optical photon to undergo specular spike (SS), specular lobe (SL), backscatter (BS) or Lambertian (L) reflection.

2.1. The surface roughness Sigmaalpha, σ_α

A rough surface is modelled as consisting of micro facets, see Fig. 1. The angle, α, of a micro-facet normal against the average surface normal is sampled from a normal distribution. The mean and standard deviation for the normal distribution are given by the average surface normal and σ_α. An increase of σ_α results in a rougher surface.

2.2. Reflectivity and reflection types

The reflectivity (R) together with the reflection type control the radiant intensity from a surface. For $R=1.0$ (default value) no optical photons are absorbed by the surface and for $R=0$ all optical photons are absorbed. If an optical photon is not absorbed Snell's law is applied using the refractive index of the two media on each side of the surface. Application of Snell's law also includes applying Fresnel's equations of reflection and refraction. Snell's law and the Fresnel equations determine if an optical photon undergoes Fresnel refraction, Fresnel reflection or total internal reflection.

There are four types of reflections: specular spike (SS), specular lobe (SL), backscatter (BS) and Lambertian (L). Fig. 2 shows the radiant intensity following SS, SL and L reflections. The GATE user defines the probability for each reflection type and the sum of the probabilities must be equal to 1.0, Lambertian reflection being implicit. SS is a reflection against the average surface normal and SL is a reflection against the normal of a micro facet. For BS the optical photon is reflected back in the incident direction.

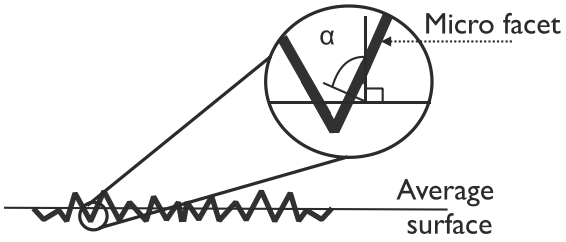

Fig. 1. A ground surface is modelled as consisting of micro facets where α is the angle of a micro-facet normal against the average surface normal.

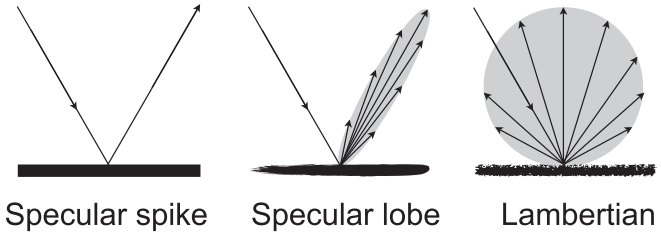

Fig. 2. For a specular spike reflection, the angle of reflection is equal to the incidence angle. For a specular lobe reflection, the angle of reflection is calculated with respect to a micro facet normal. For Lambertian (or diffuse) reflection an optical photon can be reflected into any direction in the surfaces hemisphere. The grey area and the length of the arrows indicate the radiant intensity at different reflection angles.

Lambertian reflection obeys Lambert's cosine law, i.e. the radiant intensity from a diffuse surface is directly proportional to the cosine of the angle between the observer's line of sight and the surface normal.

2.3. The dielectric–dielectric surface

The physics processes at a surface between two dielectric materials are controlled by the surface finish, the reflectivity (R) and the reflection types.

- The finish P defines a perfectly smooth surface. The GEANT4 code decides, with respect to R, if the optical photon is absorbed by the surface or reflected/refracted at the surface. In the latter case, Snell's law is applied.
- The finish G defines a rough surface and the degree of roughness is defined by σ_α. The GEANT4 code decides, with respect to R, if the optical photon is absorbed by the surface or reflected/refracted at the surface. In the latter case the angle α between the average surface normal and the micro-facet normal (see Fig. 1) is sampled and Snell's law is applied. The reflection type should be set to SS, SL, BS and/or L, where L is implicit.
- The finish PFP (GFP) defines a volume with a painted surface, e.g. a scintillator coated with a reflecting material, where R is the probability for reflection by the paint. The GEANT4 code decides, with respect to R, if the optical photon is absorbed by the paint. If not absorbed the optical photon is SS (L) reflected. No refraction occurs and Snell's law is not applied. Note: the paint is defined by the surface parameters; it is not required to define it as an additional geometrical volume.
- The finish PBP (GBP) defines a volume with a painted surface where there is a gap between a volume and paint, e.g. an imperfectly coated scintillator, where R is the probability for reflection by the paint. The refractive index for the material in the gap is defined as a surface parameter. Snell's law is applied when an optical photon reaches the boundary between the volume and the gap. If the optical photon is refracted it reaches the paint and is either absorbed or undergoes SS (L) reflection. If reflected the optical photon reaches the boundary between the gap and volume and Snell's law is applied. The optical photon can now be reflected back to the paint or refracted into the volume. Note: the paint is defined by the surface parameters; it is not required to define it as an additional geometrical volume. Illustrations of PBP and GBP surfaces can be found in Section 3.1.1, Fig. 5.

2.4. The dielectric-metal surface

The physics processes at a surface between a dielectric and a metal surface are controlled by the surface finish, the reflectivity (R), reflection type and the efficiency.

- The finish P defines a perfectly smooth reflector. The GEANT4 code decides, with respect to R, if the optical photon is absorbed by the surface or reflected at the surface. If the optical photon is reflected it undergoes SS reflection.
- The finish G defines a rough reflector. The GEANT4 code decides, with respect to R, if the optical photon is absorbed by the surface or reflected at the surface. If the optical photon is reflected, the angle α between the average surface normal and the micro-facet normal is sampled. The reflection type should be set to SS, SL, BS and/or L, where L is implicit.

Optical photons are detected by a dielectric-metal surface with efficiency >0 and $R<1.0$. If an optical photon is absorbed (all are absorbed if $R=0$), it is detected with the probability given by the surface parameter efficiency.

3. Method

All simulations were performed using GATE v6.2 with GEANT4 version 9.5 patch 01. The impact of the surface parameters was studied by simulating the energy deposition for a point source of ^{65}Zn (γ: 1115.546 keV) in a large plastic scintillator. The energy deposition was followed by the generation of optical photons, which were transported through the scintillator and then detected by a photocathode placed at one of the scintillator short ends. The surface parameters describing the scintillator surface were changed and the impact of each parameter was studied by comparing the change in the optical spectrum, i.e. the spectrum of detected optical photons per ^{65}Zn source particle depositing energy in the scintillator. For a scintillator, the optical spectrum is strongly linked to the final energy spectrum and therefore a surface parameter will also have an impact on the energy spectrum.

The plastic scintillator is part of a WBC detector system that has been previously described in Ref. Nilsson and Isakkson (2014). A schematic of the Monte Carlo model of the WBC is shown in Fig. 3. Fig. 4, redrawn from Ref. Nilsson (2014), shows an example of the output from the scintillator placed directly under the source in Fig. 3. In Fig. 4 the simulated energy spectra for a ^{137}Cs point source at source positions 30 cm and 70 cm are compared to experimental energy spectra. The processes occurring after energy deposition clearly have an impact on the spectrum resolution. Note, the experimental energy spectra were obtained using a PMT and the optical spectra studied in this article will therefore have a better resolution compared to the experimental energy spectra presented in Fig. 4.

The WBC is mainly used for detecting radionuclides with gamma energies above 1000 keV; hence ^{65}Z was used in this work.

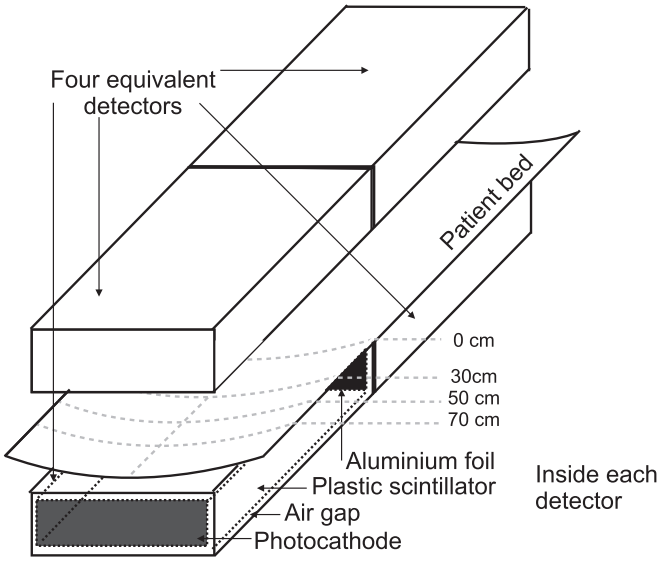

Fig. 3. A schematic of the WBC. The WBC consists of four equivalent detectors. The positions of the plastic scintillator, photocathode and aluminium foil inside each detector are indicated in the detector placed under the patient bed. The source was placed at three positions, marked by ×, along the middle of the patient bed.

3.1. The monte Carlo model of the plastic scintillator and its surfaces

All four detectors in Fig. 3 are equivalent and each detector was defined as follows: the detector housing was made of 1.0 mm stainless steel with a 0.397 mm copper window facing the patient bed. The plastic scintillator with density 1.032 g/cm^3 (Saint-Gobain Ceramics & Plastics, 2005) measured $91.5 \times 76.0 \times 25.4$ cm^3. The air gap surrounding the scintillator measured 4.8 cm between the scintillator and the copper window. A reflecting aluminium foil was placed on the short end of the scintillator. The aluminium foil measured $0.012 \times 76.0 \times 25.4$ cm^3, and its thickness was taken from the data for 3M™ Aluminium Foil Tape 425 (Riggi et al., 2010). A photocathode was placed on the opposite short end. The photocathode measured $2.5 \times 10^{-6} \times 76.0 \times 25.4$ cm^3, and its thickness was taken from Ref. Knoll (2010). The photocathode was made of the same material as the scintillator but without the scintillating properties. The patient bed was modelled as 1.0 mm thick steel plate.

The properties for the scintillator were taken from the BC-400 data sheet (Saint-Gobain Ceramics & Plastics, 2005): scintillation yield = 10, 000 optical photons per deposited MeV, absorption length = 250 cm and refractive index = 1.581. The fast time constant was set to 2.4 ns and the yield ratio to 1.0. The fast component of the light emission spectrum consisted of 7 discrete wavelengths (400, 420, 423, 440, 460, 480 and 500 nm) and their respective probabilities. The manufacturer did not provide any information for the resolution scale and Rayleigh scattering length. Here the resolution scale was set to 1.0 meaning that the standard deviation for the scintillation yield was given by (energy absorbed in MeV $\times$ 10, 000)$^{1/2}$. The Rayleigh scattering length was determined using the method described by Riggi et al. (2010).

Optical photons that left the scintillator through refraction at the scintillator–air interface were killed, i.e. they were not transported further once reaching the air. To save computational time the optical photon transport was included only for the scintillator volume placed directly under the source in Fig. 3. The sensitive detector, a GATE term to define from which volume the data is scored, was attached to the photocathode volume shown in Fig. 3.

3.1.1. The surface parameters

For each simulation three surfaces were defined: the surface between the scintillator and the air, the surface between the scintillator and the aluminium foil and the surface detecting the optical photons at the photocathode.

3.1.1.1. The aluminium foil surface. The aluminium foil surface was defined as a polished dielectric-metal surface with a detecting efficiency = 0 and SS = 1.0 (Riggi et al., 2010). R was either set equal to the reflectivity for the scintillator surface or had a wavelength dependent reflectivity as the 3M™ Aluminium Foil Tape 425, ranging from 0.865 to 0.889 (Riggi et al., 2010).

3.1.1.2. The photocathode surface. The photocathode surface (i.e. detecting surface) had the same properties in all simulations. It was defined as a polished dielectric-metal surface with $R = 0$ and SL = 1.0. The surface detecting efficiency was the same as the wavelength dependent relative efficiency for the photocathode

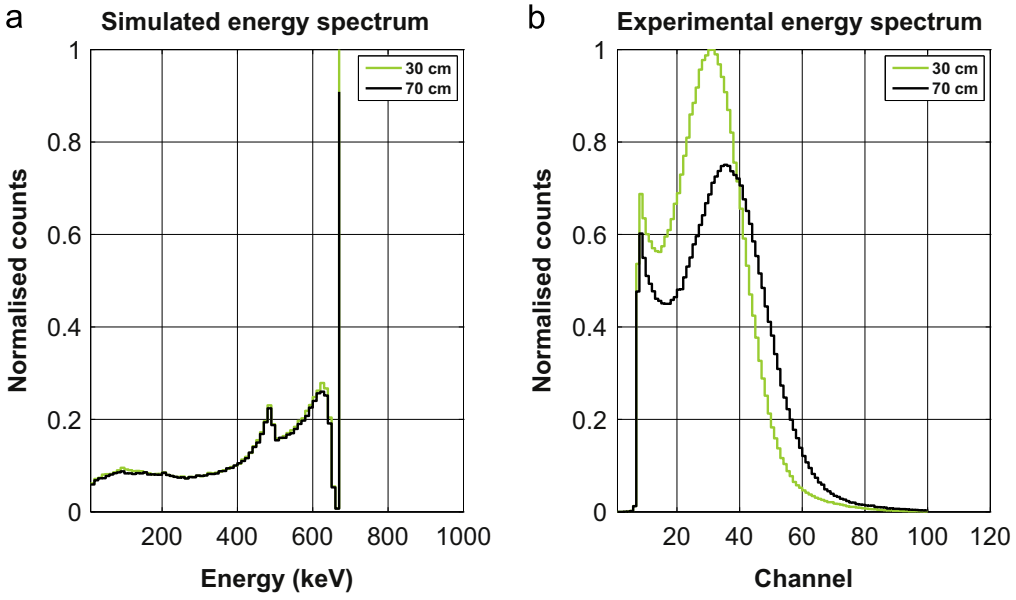

Fig. 4. (a) Simulated energy spectra for a ^{137}Cs point source at source position 30 cm and 70 cm. (b) Experimental energy spectra at the same positions as in (a). Redrawn from Ref. Nilsson (2014).

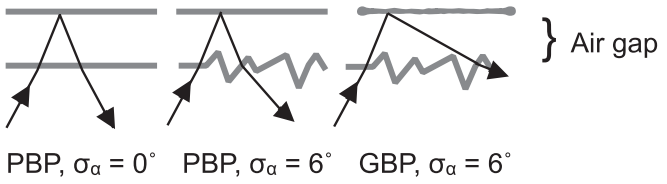

Fig. 5. An optical photon is refracted at the scintillator–air boundary. Left: polished scintillator with a perfectly reflecting paint. Middle: rough scintillator with a perfectly reflecting paint. Right: rough scintillator with a diffuse reflecting paint.

material used in the PMT EMI 9545 A (EMI Electronics Ltd.).

3.1.1.3. The scintillator surface. The scintillator surface was defined as a dielectric–dielectric surface. The impact of the reflectivity was investigated by setting R to 0.7, 0.8, 0.9 and 1.0. All reflection types (SS, SL, L and BS) and surface finish were studied and the impact of σ_α was investigated by setting σ_α=0.1°, 6° and 12° for a ground surface. For all back-painted surfaces, shown in Fig. 5, the surface refractive index was set to 1.000277 (air gap) and the reflectivity for the paint was wavelength dependent as the 3M™ Aluminium Foil Tape 425 (Riggi et al., 2010). Hence, the back-painted surfaces described a scintillator coated with aluminium foil where there was an air gap between the scintillator and the aluminium foil. The aluminium foil was either a perfect reflector (PBP) or a diffuse reflector (GBP). In total 37 different scintillator surfaces were defined, see Table 1.

3.2. The source

A point source emitting 10^6 gamma particles with energy 1115.546 keV (^{65}Zn) was placed at three positions along the middle of the patient bed, see Fig. 3. The positions, 30 cm, 50 cm and 70 cm, were measured from the centre of the WBC. For each surface listed in Table 1 three simulations were performed, one for each source position,

4. Results

All figures show the optical spectrum and the x-axis bin size is set to 30 optical photons. The reflectivity for the aluminium foil surface was either equal to the reflectivity for the scintillator surface, denoted R, or had a wavelength dependent reflectivity as the 3M™ Aluminium Foil Tape 425, denoted 3M™. In the following sections, all surfaces will be defined by a surface number as listed in Table 1 and the reflectivity for the aluminium foil. The impact of a surface parameter was quantified by calculating the shift in the optical spectrum, where the shift was defined as the displacement of the optical spectrum peak maximum. For each figure, the shifts were calculated relative to the peak maximum furthest to the right. The reference point for each surface parameter was given by the parameter value that enabled a peak maximum with highest number of detected optical photons per source particle.

4.1. The impact of the source position and the surface finish polished and ground

Fig. 6 shows the optical spectra obtained for a polished (P), ground (G), polished-front-painted (PFP) and ground-front-painted (GFP) scintillator where the ^{65}Zn source was positioned at 30 cm, 50 cm and 70 cm of the centre of the WBC. At each source position, the optical spectra shifted with the surface finish. The optical spectrum for each surface finish (P, PFP, G and GFP) shifted as the source was moved further away from the photocathode

Table 1
The scintillator surfaces. Columns 2–5 show the surface parameters for the scintillator surface, G=ground, P=polished, GBP=ground-back-painted, GFP=ground-front-painted, PBP=polished-back-painted, PFP=polished-front-painted, SL=specular lobe constant, SS=specular spike constant, BS=backscatter constant, L=Lambertian. For GBP and PBP the surface refractive index was set to 1.000277 and the reflectivity of the coating was wavelength dependent as the 3M™ Aluminium Foil Tape 425.

Surface no.	Finish	Reflectivity	σ_α (°)	Reflection type
1	G		0.1	SL=1.0
		0.7		
2	G		0.1	SL=1.0
		0.8		
3	G		0.1	SL=1.0
		0.9		
4	G		0.1	SL=1.0
		1.0		
5	G		6	SL=1.0
		0.7		
6	G		6	SL=1.0
		0.8		
7	G		6	SL=1.0
		0.9		
8	G		6	SL=1.0
		1.0		
9	G		12	SL=1.0
		0.7		
10	G		12	SL=1.0
		0.8		
11	G		12	SL=1.0
		0.9		
12	G		12	SL=1.0
		1.0		
13	G		6	SL=0.9, BS=0.1
		1.0		
14	G		6	SL=0.9, L=0.1
		1.0		
15	G		6	SL=0.9, SS=0.1
		1.0		
16	G		6	SL=0.8, BS=0.2
		1.0		
17	G		6	SL=0.8, L=0.2
		1.0		
18	G		6	SL=0.8, SS=0.2
		1.0		
19	G		6	SL=0.7, BS=0.3
		1.0		
20	G		6	SL=0.7, L=0.3
		1.0		
21	G		6	SL=0.7, SS=0.3
		1.0		
22	P		0	SS=1.0
		0.7		
23	P		0	SS=1.0
		0.8		
24	P		0	SS=1.0
		0.9		
25	P		0	SS=1.0
		1.0		
26	P		0	L=1.0
		1.0		
27	GBP		6	L=1.0
		1.0		
28	PBP		0	SS=1.0
		1.0		
29	PBP		6	SS=1.0
		1.0		
30	GFP		6	L=1.0
		0.7		
31	GFP		6	L=1.0
		0.8		
32	GFP		6	L=1.0
		0.9		
33	GFP		6	L=1.0
		1.0		
34	PFP		0	SS=1.0
		0.7		
35	PFP		0	SS=1.0

Table 1 (*continued*)

Surface no.	Finish	Reflectivity	σ_α (°)	Reflection type
		0		
36	PFP		0	SS=1.0
		0.9		
37	PFP		0	SS=1.0
		1.0		

surface (from 70 cm to 30 cm); this was most pronounced for GFP in Fig. 6(b). With respect to GFP (70 cm), the optical spectra for GFP shifted by −24% (50 cm) and −34% (30 cm).

4.2. The impact of the surface roughness, σ_α

Fig. 7 shows the optical spectra for a ground scintillator with different surface roughness, σ_α=0.1°, 6° and 12°. This is compared to an optical spectrum for a polished (P) scintillator. Each optical spectrum was obtained for the ^{65}Zn source positioned at 50 cm of the centre of the WBC. The optical spectra shifted as σ_α increased. With respect to P, the optical spectra for σ_α=6° and 12° shifted by −12% and −18%, respectively.

4.3. The impact of the reflection type

Fig. 8 shows the optical spectra for a ground scintillator where the probability for Lambertian (L) reflection was set to 0, 0.1, 0.2 and 0.3. If Lambertian reflection was not chosen the optical photons would have undergone specular lobe (SL) reflection. The optical spectra are shown for the ^{65}Zn source positioned at 30 cm, 50 cm and 70 cm of the centre of the WBC. Fig. 9 shows the optical spectra for a ground scintillator where the probability for backscatter (BS) was set to 0, 0.1, 0.2 and 0.3. If backscatter reflection was not chosen, the optical photons would have undergone SL reflection. The optical spectra are shown for the ^{65}Zn source positioned at 30 cm, 50 cm and 70 cm of the centre of the WBC.

The optical spectra in Figs. 8 and 9 shifted as the probability for L and BS increased, this was slightly more noticeable in Fig. 8. For the source position 50 cm, the optical spectra shifted, with respect to SL=1.0, by −11% (L=0.9), −21% (L=0.8) and −29% (L=0.7) compared to −9% (BS=0.9), −18% (BS=0.8) and −27% (BS=0.7).

Simulations were also done for a ground scintillator where the probability for specular spike (SS) reflection was set to 0, 0.1, 0.2 and 0.3. If specular spike reflection was not chosen, the optical photons would have undergone SL reflection. There was barely any change in optical spectra as the probability for SS increased, i.e. the optical spectra overlapped with SS=0.

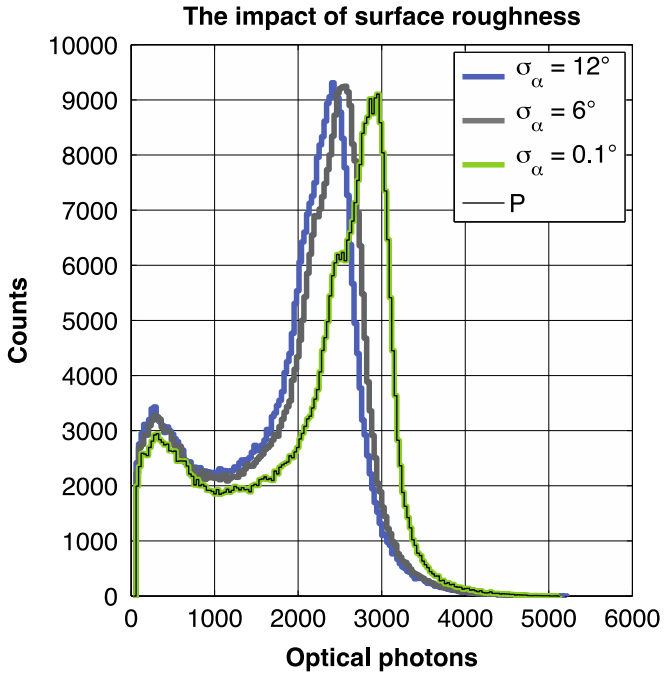

Fig. 7. The optical spectra for a ground scintillator with different surface roughness, σ_α=12° (12_R), 6° (8_R) and 0.1° (4_R). This is compared to an optical spectrum for a polished scintillator (25_R). Each optical spectrum was obtained for the ^{65}Zn source positioned at 50 cm.

4.4. The impact of the scintillator surface reflectivity

Fig. 10 shows the optical spectra for a polished scintillator with the reflectivity *R* set to 0.8, 0.9 and 1.0. The optical spectra are shown for the ^{65}Zn source positioned at 30 cm, 50 cm and 70 cm of the centre of the WBC.

The optical spectra shifted as R decreased and the shift due to

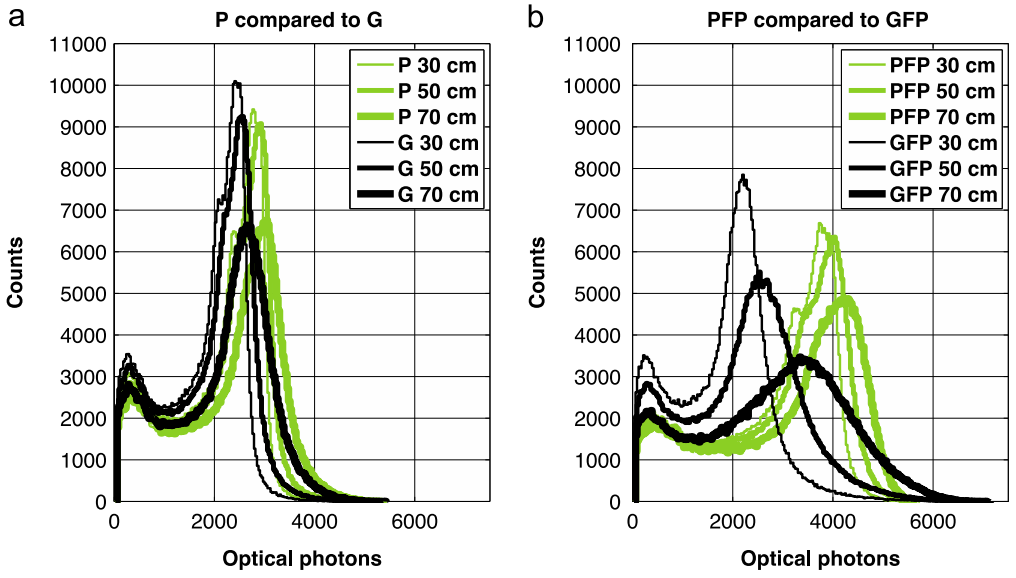

Fig. 6. (a) The optical spectra for a polished scintillator (25_R) and a ground scintillator (8_R). (b) The optical spectra for a polished-front-painted scintillator (37_R) and ground-front-painted scintillator (33_R). The optical spectra were simulated at source positions 30 cm, 50 cm and 70 cm for each surface finish.

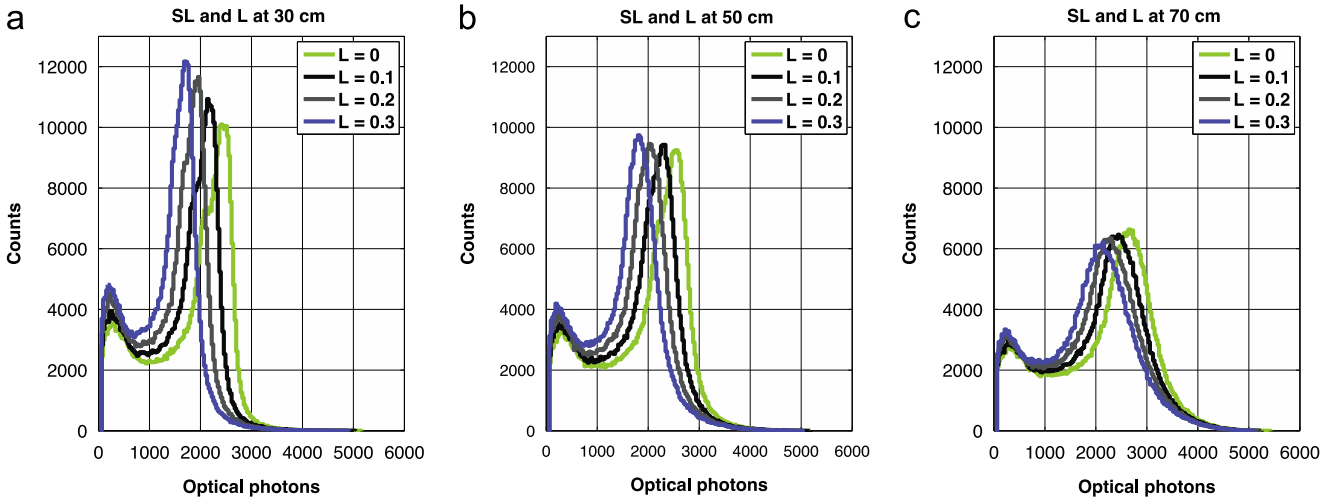

Fig. 8. (a–c) The optical spectra for a ground scintillator where the probability for Lambertian reflection is set to 0 (8_R), 0.1 (14_R), 0.2 (17_R) and 0.3 (20_R).

source position increased as R decreased. For the source position 70 cm and $R=1.0$, the optical spectrum shifted by –4% (50 cm) and –9% (30 cm); for the source position 70 cm and $R=0.8$ the optical spectrum shifted by –11% (50 cm) and –16% (30 cm). Simulations were also done for a ground scintillator with R set to 0.8, 0.9 and 1.0 (not shown). The optical spectra for the ground surface behaved as the optical spectra presented in Fig. 10, but with a slightly greater shift due to the source position. For the ground surface and the source position 70 cm and R = 1.0, the optical spectrum shifted by –3% (50 cm) and –9% (30 cm); for the source position 70 cm and $R=0.8$ the optical spectrum shifted by –15% (50 cm) and –21% (30 cm).

4.5. The impact of back-painted surfaces

Fig. 11 shows the optical spectra for a ground (G with $\sigma_\alpha=6°$) and a polished (P) scintillator. This is compared to a polished scintillator with a perfectly reflecting paint (PBP and $\sigma_\alpha=0°$), a ground scintillator with a perfectly reflecting paint (PBP and $\sigma_\alpha=6°$), a ground scintillator with a diffuse reflecting paint (GBP and $\sigma_\alpha=6°$) and a polished scintillator with a perfectly reflecting paint (PBP and $\sigma_\alpha=0°$), see Fig. 5. The optical spectra are shown for the ^{65}Zn source positioned at 30 cm, 50 cm and 70 cm of the centre of the WBC.

For the perfectly reflective paint, the optical spectrum shifted slightly when the scintillator surface was changed from polished to ground. For the source position 50 cm, the optical spectrum shifted by –2% for PBP and $\sigma_\alpha=6°$ relative to PBP and $\sigma_\alpha=0°$. The shift increased further when the perfectly reflecting paint was changed to a diffuse reflecting paint. For the source position 50 cm, the optical spectrum shifted by –10% for GBP and $\sigma_\alpha=6°$ relative to PBP and $\sigma_\alpha=0°$. When the paint was removed, for the source position 50 cm, the optical spectrum shifted by –13% for P and –24% for G relative to PBP and $\sigma_\alpha=0°$.

4.6. Benchmarking

A comparison between simulated energy spectrum and experimental energy spectrum, obtained using the WBC system, for the radionuclides ^{137}Cs, ^{54}Mn and ^{65}Zn can be found in Ref Nilsson and Isaksson (2015). The simulated energy spectrum showed a very good agreement to the experimental energy spectrum for low dead time measurements. The relative position of the peak maxima for the simulated spectrum corresponded to relative position of the peak maxima for the experimental energy spectra and the simulated counting efficiency (counts per second / Bq) differed with 1–10% compared to the experimental counting efficiency.

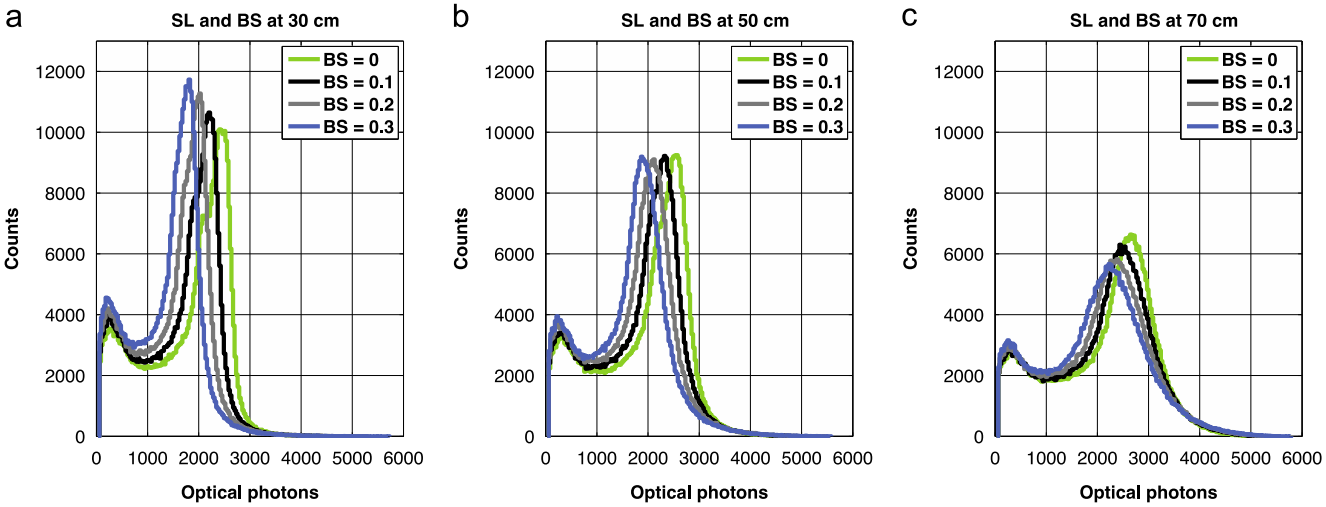

Fig. 9. (a–c) The optical spectra for a ground scintillator where the probability for backscatter is set to 0 (8_R), 0.1 (13_R), 0.2 (16_R) and 0.3 (19_R).

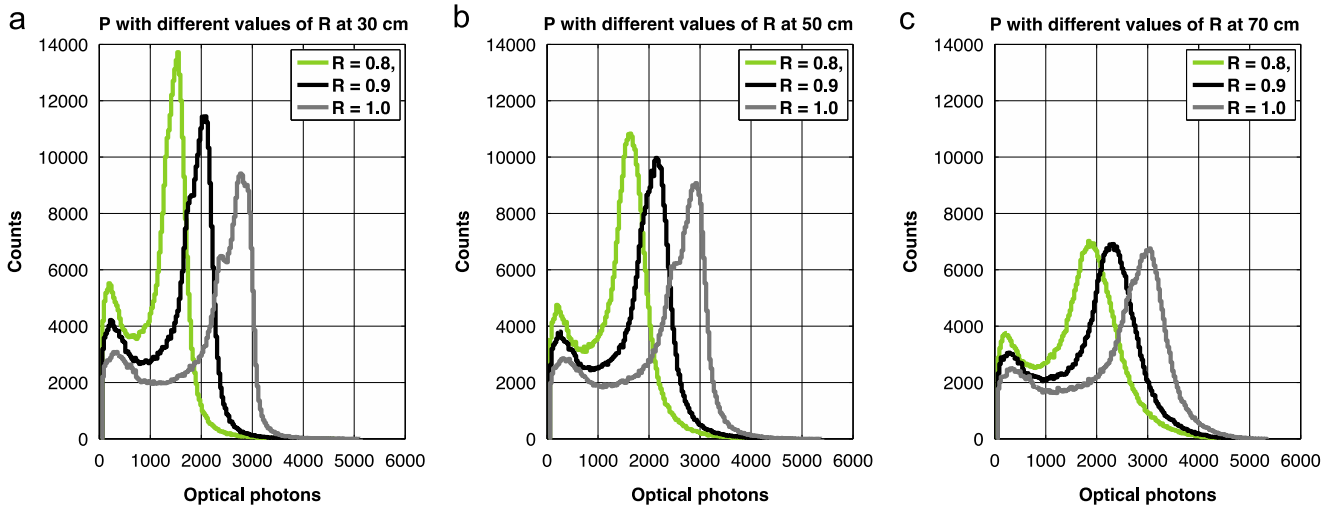

Fig. 10. (a–c) The optical spectra for a polished scintillator with different values of the reflectivity: R=0.8 (23_R), 0.9 (24_R) and 1.0 (25_R).

5. Discussion

In this work the optical spectrum for a large plastic scintillator was investigated. Compared to a plastic (organic) scintillator, an inorganic scintillator is better suited for spectrometry due to higher light yield (Knoll, 2010) and higher probability for photoelectric absorptions of high-energy gamma photons (Siciliano et al., 2008). An optical spectrum from a plastic scintillator has a poorer energy resolution compared to the spectrum from an inorganic scintillator of the same size. However, the processes controlled by the surface parameters are not dependent on the scintillator material, e.g. if the reflectivity type is changed from specular lobe to Lambertian, the optical spectrum will shift regardless if the scintillator is organic or inorganic. The discussion and conclusions made in this work are therefore applicable to organic as well as inorganic scintillators of different sizes and shapes.

5.1. The impact of the source position and the difference between the surface finish polished and ground

Fig. 6 shows the optical spectra for a scintillator with a polished, ground, polished-front-painted (PFP) or ground-front-painted (GFP) surface. For a PFP or GFP surface, all optical photons were reflected and could only be lost through bulk absorption in the scintillator or through absorption (but no detection) by the photocathode surface. The probability for bulk absorption increases with the distance travelled by an optical photon in the scintillator, which explains why the shift increased as the source was moved away from the photocathode surface. Riggi et al. (2010) have shown that a ground surface leads to a more erratic optical photon path. A shorter effective path increases the probability for an optical photon to be absorbed by the bulk before reaching the photocathode surface, which explains the shift of the optical spectrum for a GFP surface relative to a PFP surface.

For a polished or ground scintillator, optical photons could be lost through three processes: bulk absorption in the scintillator, absorption (but no detection) by the photocathode surface or leaving the scintillator through refraction at the scintillator–air boundary. By including refraction, the impact of bulk absorption on the optical spectrum decreases. Fig. 6 shows that a perfectly coated scintillator (PFP and GFP) may actually cause a broadening of an optical spectrum if the scintillator is large with respect to its absorption length.

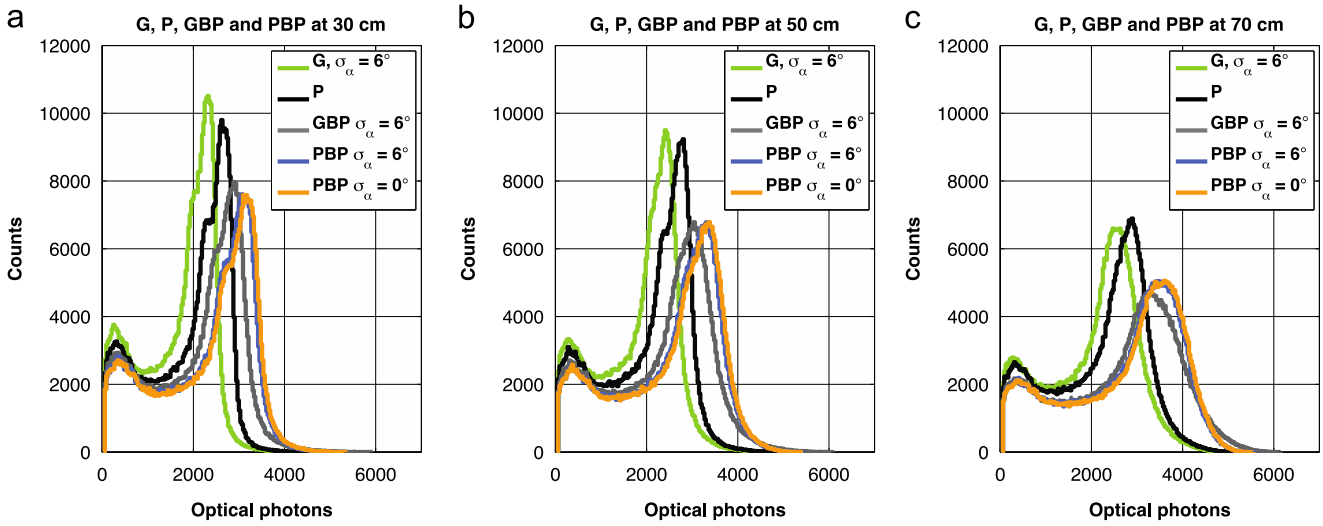

Fig. 11. (a–c) The optical spectra for a ground scintillator (8_3M™) and a polished scintillator (25_3M™) compared to ground and polished scintillator with different coatings; a polished scintillator with a perfectly reflective coating (28_3M™), a ground scintillator with diffuse reflective coating (29_3M™) and a ground scintillator with a diffuse reflecting coating (27_3M™).

5.2. The impact of the surface roughness, σ_α

Fig. 7 shows the optical spectra for a ground scintillator with an increasing surface roughness. Previously reported values for σ_α is in the range 0–13.4° (Riggi et al., 2010; Janecek and Moses, 2008, 2010; Nozka et al., 2011; van der Laan et al., 2010) and the values used in this work (0.1°, 6 ° and 12°) described respectively a nearly perfectly polished scintillator, a rough scintillator and a very rough scintillator. The reflection angle for a ground surface is sampled from a normal distribution with standard deviation given by σ_α. An increase of σ_α results in a rougher surface. Hence, as σ_α increases the optical spectrum shifts since a rougher surface leads to a more erratic path for the optical photons. More optical photons are then absorbed by the scintillator or lost through refraction at the plastic scintillator–air boundary before reaching the photocathode. The greatest shift was seen when σ_α increased from 0.1° to 6°. A further increase of σ_α, from 6° to 12°, had a smaller impact on the optical spectrum. If a ground surface is "rough enough" the surface roughness parameter σ_α has a minor impact on the optical spectrum, and hence a minor impact on an energy spectrum. The meaning of minor impact is expanded further in the end of Section 5.3.

5.3. The impact of the reflection type

Fig. 8 shows the optical spectra for a scintillator where an optical photon either underwent specular lobe (SL) or Lambertian (L) reflection. Fig. 9 shows the optical spectra for a scintillator where an optical photon either underwent specular lobe (SL) or backscatter (BS) reflection. Fig. 8 shows that the optical spectrum shifted as the probability for Lambertian reflection increased. A Lambertian reflection results in a more erratic path for the optical photons compared to specular lobe reflection, see Fig. 2. As the probability for Lambertian reflection increases, more optical photons are lost either through bulk absorption or refraction at the scintillator–air boundary before reaching the photocathode. A similar behaviour can be seen in Fig. 9, i.e. the shift in the optical spectra increase as the probability for backscatter increases. Backscatter reflection is more constrained compared to Lambertian reflection, resulting in a less erratic path for the optical photons. This results in more optical photons reaching the photocathode and a slight smaller shift of the optical spectra shown in Fig. 9 compared to Fig. 8.

When the reflectivity type was set to a combination of specular lobe (SL) and specular spike (SS) reflection, there was barely any noticeable difference between setting SL to 1.0 and SL to 0.7. The radiant intensity from a rough surface can be modelled as consisting of components from both specular spike and specular lobe reflection (Nayar et al., 1991), but from an optical/energy spectrum point of view, the specular spike component has a negligible impact on spectrum resolution when $SS \leq 0.3$.

Increasing the probability for Lambertian or backscatter reflection had a similar impact on the optical spectrum as increasing σ_α; the optical spectrum shifted since the distribution of reflection angles resulted in a more erratic optical photon path. Hence, for a ground surface, both σ_α and the reflectivity type control the shifts in an optical spectrum caused by the erratic optical photon path. Of these two, the reflectivity type was shown to have the greatest impact. In Figs. 8 and 9, all optical spectra were obtained with $\sigma_\alpha=6°$. The shifts due to a change in the probability type were rather large, at most −29% for SL=0.7 and $L=0.3$. In comparison, Fig. 7 showed that an increase of σ_α resulted in a rather small shift, −6% between $\sigma_\alpha=6°$ and $\sigma_\alpha=12°$.

5.4. The impact of the scintillator surface reflectivity

Fig. 10 shows the optical spectra for a polished scintillator with a different value of the reflectivity (R), the probability for an optical photon to not be absorbed by the surface. The optical spectra in Fig. 10 shifted as the reflectivity decreased since more optical photons were lost through surface absorption.

5.5. The impact of back-painted surfaces

Fig. 11 shows the optical spectra for a polished (P) or ground (G) scintillator surface. This is compared to the optical spectra for a scintillator painted with a diffuse reflector (GBP) or a perfect reflector (PBP), where there is an air gap between the scintillator and the paint. For the back-painted surfaces, G and P in GBP and PBP relate to the paint and describe if the reflector is perfect or diffuse. The finish of the painted volume, in this case the scintillator, is defined by σ_α, where $\sigma_\alpha=0°$ defines a polished scintillator and $\sigma_\alpha=6°$ a ground scintillator. For an unpainted scintillator, an optical photon leaving the scintillator through refraction was lost from the signal. For a painted scintillator, an optical photon leaving the scintillator through refraction could re-enter the scintillator volume, if reflected by the paint and then refracted from the air gap into the scintillator.

For the perfectly reflective paint there was a small shift in the optical spectrum when the scintillator surface was changed from polished to ground, from PBP with $\sigma_\alpha=0°$ to PBP with $\sigma_\alpha=6°$. This is explained by the optical photon's more erratic path caused by reflections against a ground surface. For the same reason, the shift in the optical spectrum became more pronounced when the paint for the ground scintillator was changed from perfect reflector to a diffuse reflector, from PFP with $\sigma_\alpha=6°$ to GBP with $\sigma_\alpha=6°$. The optical spectrum shifted further more as the paint was removed because the optical photons that left the scintillator though refraction could not be reflected back into the scintillator volume.

The difference between a painted scintillator with and without a gap between the paint and the scintillator (front-painted and back-painted surfaces) can be studied in Figs. 6(b) and 11. An interesting observation for ground-painted surfaces is that the air gap improves the resolution for the optical spectrum at source positions 50 cm and 70 cm. For a GFP surface all optical photons reaching the scintillator surface undergo Lambertian reflection. For a GBP surface, when an optical photon reaches the scintillator surface Snell's law is applied with respect to the refractive indices of the scintillator and air. The optical photons are reflected with respect to the scintillator surface, in this case a ground surface since $\sigma_\alpha=6°$. The refracted optical photons pass the air gap, reach the paint and, if not absorbed, undergo Lambertian reflection. The optical photon can then re-enter the scintillator through refraction at the air–scintillator boundary. For the GBP surface the reflected optical photons underwent specular lobe or Lambertian reflection whereas all optical photons underwent Lambertian reflection for the GFP surface, hence resulting in a more erratic path for the optical photons.

For a back-painted surface it is important to know if the paint is a perfect or diffuse reflector whereas the roughness of the volume–gap interfaces is of minor importance. The latter has a small impact on the optical spectrum and hence a small impact on an energy spectrum and its resolution.

5.6. Benchmarking

Fig. 4 shows a comparison between simulated energy deposition spectrum and experimental energy spectrum for a ^{137}Cs source obtained using the WBC modelled in this work. As stated in Section 3, the signal from the scintillator was further amplified

with a PMT for the experimental spectrum. By adding PMT modelling to the Monte Carlo model of the WBC, the simulated spectrum is equivalent to an experimental energy spectrum. Simulated energy spectrum for the WBC, obtained for ^{137}Cs, ^{54}Mn and ^{65}Zn, were benchmarked in Ref. Nilsson and Isaksson (2015). The work presented in this article, and in Refs. Nilsson and Isaksson (2015) and Nilsson (2014) makes it possible to understand what causes the differences between the simulated energy deposition spectrum in Fig. 4a and the experimental energy spectrum in Fig. 4b.

A ground surface finish was used for the scintillators of the WBC in Refs. Nilsson and Isaksson (2015) and Nilsson (2014). The optical spectrum has a relatively short right tail compared to the experimental spectrum in Fig. 4b. The right tail is seen in a simulated energy spectrum first after PMT modelling has been included (Nilsson and Isaksson, 2015; Nilsson, 2014). The smeared Compton edge is due to both PMT modelling and optical transport, it is clearly seen in the simulated energy deposition spectrum in Fig. 4a but barely noticeable in the optical spectrum for a ground surface in Fig. 5. The shifts of the peak maxima with the source position in the experiment spectrum were due to the optical transport and the left tail of the experimental energy spectrum are caused by the energy deposition and the following optical transport.

5.7. About the optical transport in GATE

The aim of this work was to study each surface parameter and its impact on an optical spectrum. The usefulness of including optical transport, when simulating the response from the large plastic scintillators described in this work, is shown in Ref. Nilsson and Isaksson (2015). For anyone interested in optical transport models and their verifications, the following articles are of great use. A general description of GATE has been written by Jan et al. (2011', 2004). van der Laan et al. (2010) have written an article about the verification of the optical transport in GATE/GEANT4 and how to experimentally determine the optical parameters. Nayar et al. (1991) have made a detailed study of reflectance models based on physical and geometrical optics. The UNIFIED model used in GATE/GEANT4 was first described by Levin and Moisan (1997). Janecek and Moses (2008, 2010) have shown that the probability for the four reflection types (see Section 2.2) is not independent of the incident angle of the optical photons. A description of optical transport and transport models has been published by Bea et al. (1994), who also compared experimental data to simulated data using an in-house code. Riggi et al. (2010', 2011) have published two comprehensive studies about simulating optical transport in plastic scintillators using GEANT4. Janecek and Moses (2010) and Roncali and Cherry (2013) have proposed a method where the physics processes an optical photon undergoes at a surface is determined using measured data instead of calculating the physics processes using a theoretical model of the surface. Both works showed a good agreement to experimental data but the method has not yet been incorporated in the standard GATE and GEANT4 simulation toolkits.

6. Conclusions

The usefulness and importance of including optical transport for scintillators used for spectrometry has been shown. A simulated energy deposition spectrum differs drastically from an experimental energy spectrum; the experimental spectrum is sensitive to the source position and shows a decreased energy resolution. By including optical transport in the simulations both the source position sensitivity and decrease in energy resolution were observed in the optical spectrum, i.e. the output from a scintillator. An optical spectrum shows the lowest limit of achievable energy resolution for a scintillator and any alteration of the surface parameters will ultimately influence the energy spectrum.

The surface parameter finish was shown to have the greatest impact on the optical spectrum whereas the surface parameter controlling its roughness, σ_α, was shown to have the smallest impact. A change in the optical spectrum will ultimately have an impact on a simulated energy spectrum. By studying the optical spectra presented in this work, a GEANT4 user can predict the shift in an optical spectrum caused be the alteration of a specific surface parameter.

Acknowledgements

This project was financed by the Swedish Civil Contingencies Agency (Grant no. dnr 2011-870). The authors would also like to thank Peter Gumplinger for answering question about the optical transport in GEANT4.

Appendix A. Supplementary information

Supplementary data associated with this article can be found in the online version at http://dx.doi.org/10.1016/j.apradiso.2015.04.017.

References

Bea, J., Gadea, A., Garciaraffi, L.M., Rico, J., Rubio, B., Tain, J.L., 1994. Nucl. Instrum. Methods A 350, 184.
EMI Electronics Ltd. Valve Division. EMI Photomultiplier Tubes, Brochure ref.: 30M/6-67 (PMT) Issue 1.
GATE, 2013. Users Guide v6.2. ⟨http://wiki.opengatecollaboration.org⟩ (accessed 31.01.13).
GEANT4, 2012a. User's Guide for Application Developers Version 9.6.0. ⟨http://geant4.web.cern.ch⟩ (accessed 30.11.12).
GEANT4, 2012b. Physics Reference Manual Version 9.6.0. ⟨http://geant4.web.cern.ch⟩ (accessed 30.11.12).
International Commission on Radiological Protection, 2009. ICRP Publication 110. Annals of the ICRP 39.
Jan, S., Benoit, D., Becheva, E., Carlier, T., Cassol, F., Descourt, P., Frisson, T., Grevillot, L., Guigues, L., Maigne, L., Morel, C., Perrot, Y., Rehfeld, N., Sarrut, D., Schaart, D. R., Stute, S., Pietrzyk, U., Visvikis, D., Zahra, N., Buvat, I., 2011. Phys. Med. Biol. 56, 881.
Jan, S., Santin, G., Strul, D., Staelens, S., Assie, K., Autret, D., Avner, S., Barbier, R., Bardies, M., Bloomfield, P.M., Brasse, D., Breton, V., Bruyndonckx, P., Buvat, I., Chatziioannou, A.F., Choi, Y., Chung, Y.H., Comtat, C., Donnarieix, D., Ferrer, L., Glick, S.J., Groiselle, C.J., Guez, D., Honore, P.F., Kerhoas-Cavata, S., Kirov, A.S., Kohli, V., Koole, M., Krieguer, M., van der Laan, D.J., Lamare, F., Largeron, G., Lartizien, C., Lazaro, D., Maas, M.C., Maigne, L., Mayet, F., Melot, F., Merheb, C., Pennacchio, E., Perez, J., Pietrzyk, U., Rannou, F.R., Rey, M., Schaart, D.R., Schmidtlein, C.R., Simon, L., Song, T.Y., Vieira, J.M., Visvikis, D., de Walle, R.V., Wieers, E., Morel, C., 2004. Phys. Med. Biol. 49, 4543.
Janecek, M., Moses, W.W., 2008. IEEE Trans. Nucl. Sci. 55, 2432.
Janecek, M., Moses, W.W., 2010. IEEE Trans. Nucl. Sci. 57, 964.
Knoll, G.F., 2010. Radiation Detection and Measurement, 4th ed. John Wiley, Hoboken, N.J..
Levin, A., Moisan, C., 1997. IEEE Nucl. Sci. Symp. Conf. Rec. 2, 702.
Nilsson, J., Isaksson, M., 2015. Radiat. Prot. Dosim. 163, 458.
Nilsson, J., Isakkson, M., 2014. Prog. Nucl. Sci. Technol. 4, 427.
Nilsson, J., 2014. Modeling of Radiative Processes in Organic Scintillators (Ph.D. thesis). University of Gothenburg, Sweden, ISBN: 978-91-628-8938-8.
Nozka, L., Pech, M., Hiklova, H., Mandat, D., Hrabovsky, M., Schovanek, P., Palatka, M., 2011. Opt. Express 19, 4199.
Nayar, S.K., Ikeuchi, K., Kanade, T., 1991. IEEE Trans. Pattern Anal. 13, 611.
Pelowitz, D., 2008. MCNPX, User's Manual Version 2.6.0., LA-CP-07-1473. Los Alamos National Laboratory.
Riggi, S., La Rocca, P., Leonora, E., Lo Presti, D., Pappalardo, G.S., Riggi, F., Russo, G.V., 2010. Nucl. Instrum. Methods A 624, 583.
Riggi, S., La Rocca, P., Riggi, F., 2011. Eur. J. Phys. 32, 329.
Roncali, E., Cherry, S.R., 2013. Phys. Med. Biol. 58, 2185.
Saint-Gobain Ceramics & Plastics, 2005. BC-400, BC-404, BC-408, BC-412, BC-416 Premium Plastic Scintillators.
Siciliano, E.R., Ely, J.H., Kouzes, R.T., Schweppe, J.E., Strachan, D.M., Yokuda, S.T., 2008. Nucl. Instrum. Methods A 594, 232.
van der Laan, D.J., Schaart, D.R., Maas, M.C., Beekman, F.J., Bruyndonckx, P., van Eijk, C.W.E., 2010. Phys. Med. Biol. 55, 1659.